ACS Catalysis

Research Article

pubs.acs.org/acscatalysis

Mechanism of Initiation in the Phillips Ethylene Polymerization Catalyst: Redox Processes Leading to the Active Site

Carole Brown,[†] J. Krzystek,[‡] Randall Achey,[†] Adrian Lita,[†] Riqiang Fu,[‡] Robert W. Meulenberg,[§] Matthew Polinski,[†] Nathan Peek,[†] Youhong Wang,[∥] Lambertus J. van de Burgt,[†] Salvatore Profeta, Jr.,[†] A. E. Stiegman,*[,†] and Susannah L. Scott*[,∥]

[†]Department of Chemistry and Biochemistry, Florida State University, Tallahassee, Florida 32306, United States

[‡]National High Magnetic Field Laboratory, Tallahassee, Florida 32310, United States

[§]Department of Physics and Astronomy, University of Maine, Orono, Maine 04469, United States

[∥]Department of Chemical Engineering, University of California, Santa Barbara, California 93106, United States

Supporting Information

ABSTRACT: The detailed mechanism by which ethylene polymerization is initiated by the inorganic Phillips catalyst (Cr/SiO_2) without recourse to an alkylating cocatalyst remains one of the great unsolved mysteries of heterogeneous catalysis. Generation of the active catalyst starts with reduction of Cr^{VI} ions dispersed on silica. A lower oxidation state, generally accepted to be Cr^{II}, is required to activate ethylene to form an organoCr active site. In this work, a mesoporous, optically transparent monolith of Cr^{VI}/SiO_2 was prepared using sol−gel chemistry in order to monitor the reduction process spectroscopically. Using in situ UV−vis spectroscopy, we observed a very clean, stepwise reduction by CO of Cr^{VI} first to Cr^{IV}, then to Cr^{II}. Both the intermediate and final states show XANES consistent with these oxidation state assignments, and aspects of their coordination environments were deduced from Raman and UV−vis spectroscopies. The intermediate Cr^{IV} sites are inactive toward ethylene at 80 °C. The Cr^{II} sites, which have long been postulated as the end point of CO reduction, were observed directly by high-frequency/high-field EPR spectroscopy. They react quantitatively with ethylene to generate the organoCr^{III} active sites, characterized by X-ray absorption and UV−vis spectroscopy, which initiate polymerization.

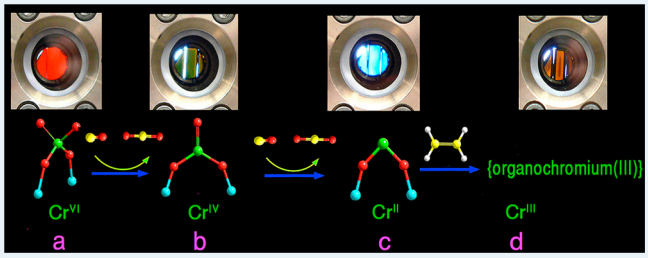

KEYWORDS: *Phillips catalyst, ethylene polymerization, active site, heterogeneous catalyst, sol−gel, reaction mechanism, redox activation, in situ spectroscopy*

INTRODUCTION

The Phillips ethylene polymerization catalyst has been used successfully in the commercial production of high-density polyethylene (HDPE) for over six decades, starting from its serendipitous discovery by Hogan and Banks at Phillips Petroleum in 1951.[1,2] Even today, it is responsible for producing as much as 50% of the world's annual HDPE output of 30 million tons.[2] Due to its industrial importance, the Phillips catalyst has been studied extensively, and many of the operating parameters that affect its activity and the properties of the polyethylene it produces are well documented.[2−4] The catalyst is a supported metal oxide, made by dispersing Cr^{VI} ions on an amorphous silica support. It is typically synthesized by wet impregnation of a silica gel with Cr ions, at loadings that are commonly about 1.0 wt % (corresponding to 1.2 mol % Cr). In the original method, CrO_3 was used as the Cr source, but its toxicity soon led to its replacement by more benign Cr^{III} compounds.[2] After impregnation, the Cr-modified silica is dried and calcined at high temperature (>500 °C), causing complete oxidation to Cr^{VI}, which is a precursor of the active oxidation state.

The isolated Cr^{VI} sites have been structurally characterized using X-ray absorption fine structure (XAFS) and vibrational spectroscopies, and modeled using DFT methods.[5−8] The dominant species is a chromate ester with two anchoring Cr−O−Si bonds and two terminal Cr═O bonds (Scheme 1a). The first step in the activation of the precatalyst is the reduction of the supported Cr^{VI} sites. In industrial practice, this is achieved by exposure to either ethylene or CO at slightly elevated temperatures (80−120 °C), and the reduced sites are formed in situ during a prolonged induction period. Catalyst reduction by CO is often preferred in laboratory studies, because it allows the resulting sites to be studied without the complications of ensuing polymerization. Both activation procedures generate highly active catalysts and produce very similar polymers.[2,9,10] Regardless of the reduction method, the final oxidation state is accepted to be Cr^{II}.[2] Due to the very high reactivity of the fully reduced catalyst, it has generally been characterized only

Received: May 4, 2015
Revised: August 7, 2015
Published: August 13, 2015

DOI: 10.1021/acscatal.5b00927
ACS Catal. 2015, 5, 5574−5583

Scheme 1. Oxidation States of the Phillips Catalyst and Colors Observed Sequentially during Its CO Reduction[a]

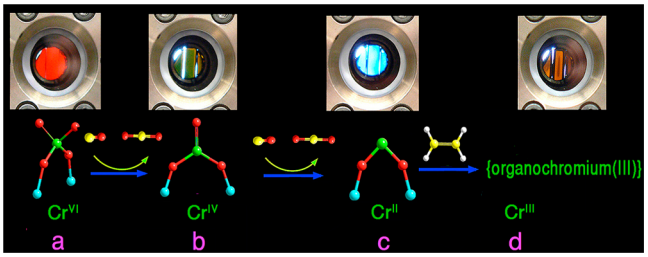

[a](a) Initial Cr^{VI} state; (b) the partially reduced Cr^{IV} state (230 °C); (c) the fully reduced Cr^{II} state (350 °C); and (d) the Cr^{III} state formed after evacuation of CO, upon reaction with ethylene (80 °C).

indirectly, particularly in early studies.[9,10] The Cr^{II} sites are regarded as precursors of the active sites, which form upon reaction of Cr^{II} with ethylene. Neither the structure nor the oxidation state of the resulting active sites has been directly characterized, although several organoCr^{IV} species, arising from two-electron oxidation of Cr^{II} by ethylene, have been inferred from IR spectra, or otherwise posited.[2,11,12] The mechanism of the initial reaction of ethylene with Cr^{II} remains elusive. Recently, minor Cr^{III} sites present in the reduced catalyst were proposed to be responsible for forming organoCr^{III} active sites without a redox reaction, by invoking ethylene deprotonation.[13,14] This suggestion, which explicitly excludes participation of Cr^{II} in the activation process, has been shown to be based on flawed analyses of IR and DFT results[15] and is contrary to a large body of prior results.[2]

In this study, we report a stepwise investigation of the CO reduction pathway leading to the activated Cr^{II} precatalyst. The latter was observed directly using high-field/high-frequency EPR spectroscopy. We also provide experimental confirmation that the Cr^{II} precatalyst reacts with ethylene in a redox process to form a new species active toward the polymerization of ethylene.

RESULTS AND DISCUSSION

Preparation of Cr/SiO_2. The Phillips catalyst used in this study was made in the form of sol–gel monoliths, consisting of porous silica containing highly dispersed Cr^{VI} ions (see Figure 1). They were synthesized using established multicomponent sol–gel techniques[14,15] and calcined in air at 500 °C. Once sealed in the spectroscopic cell, the monoliths were calcined yet again at 500 °C under dry oxygen (see Supporting Information).[16,17] The application of such monoliths in our investigation of the Phillips mechanism builds on our earlier work, in which we pioneered their use in spectroscopic studies of a variety of silica-supported catalysts.[5,18−21] In particular, their optical transparency provides significant advantages over powdered catalysts for the spectroscopic characterization of metal oxide active sites, whereas their porosity allows molecular reactants to diffuse to the reactive sites and form intermediates. As fabricated, the monoliths are mesoporous, with an average pore size and pore volume of 2.9 nm and 0.26 cm^3/g, respectively (Figure S1). The combined accessibility of high quality UV–vis spectra and reactivity measurements can be exceptionally useful in elucidating reaction mechanisms involving highly dispersed transition metal ions.[22]

Reduction of Cr^{VI} to Cr^{IV}. It is well-known that active Phillips catalysts can be generated by reducing Cr^{VI}/SiO_2 with CO at temperatures from 300 to 400 °C.[23] In our experiments, reduction was carried out under flowing CO at atmospheric pressure while monitoring changes in the UV–vis spectrum of the calcined Cr^{VI}/SiO_2 xerogel. Spectra were monitored in transmission mode as a function of temperature, using a high-temperature/high-pressure spectroscopic cell (Figure S2). In an initial experiment, the temperature of the monolith was increased until the UV–vis spectrum began to change, at ca. 230 °C. In a subsequent experiment, the temperature was held constant at 230 °C under flowing CO, causing the color of the monolith to change from orange to green (Scheme 1a,b). The isothermal UV–vis spectra reveal an extremely clean transformation, with a well-defined isosbestic point at 550 nm and the emergence of a new peak at 720 nm (Figure 2a). After 14 h at this temperature, no further changes were observed.

Reduction of Cr^{VI} by CO was reported previously at approximately this temperature,[24] although with no indication

Figure 1. Optically transparent Cr^{VI}/SiO_2 sol–gel monoliths, fabricated by sol–gel chemistry for use in ethylene polymerization experiments.

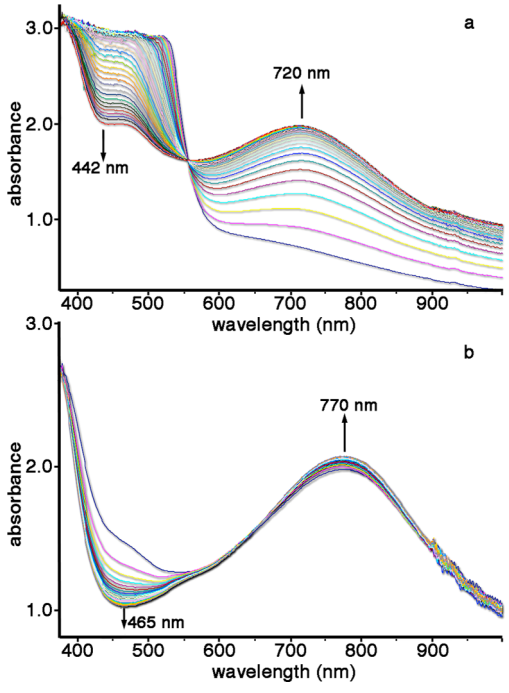

Figure 2. UV–vis spectroscopic changes observed during isothermal reduction of a Cr^{VI}/SiO_2 xerogel (0.5 mol % Cr) with flowing CO at ambient pressure: (a) at 230 °C; then (b) at 350 °C.

DOI: 10.1021/acscatal.5b00927
ACS Catal. 2015, 5, 5574−5583

that the reaction proceeds as cleanly as is apparent in Figure 2a. The oxidation state of the Cr species formed at 230 °C was investigated by X-ray absorption near-edge spectroscopy (XANES). Figure 3 shows the Cr *K*-edge located at 6004.4

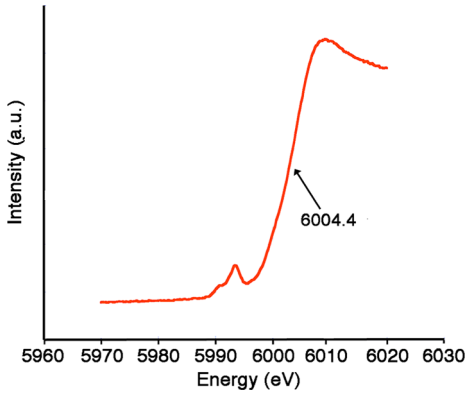

Figure 3. Cr *K*-edge XANES of Cr^{IV}/SiO_2, prepared by CO reduction of Cr^{VI}/SiO_2 (0.5 mol % Cr) at 230 °C, with the energy referenced to a Cr foil standard (5989.2 eV).

eV, suggesting the presence of Cr^{IV} by comparison to a reference material (*bis*(neopentyl)Cr^{IV}/SiO_2, 6004.2 eV), and consistent with prior observations made by Krauss et al.[25,26] The first step of the process is therefore inferred to be the reduction of Cr^{VI} to Cr^{IV}, depicted as the transformation of $(\equiv SiO)_2Cr^{VI}O_2$ to $(\equiv SiO)_2Cr^{IV}O$ in Scheme 1a,b. When briefly exposed to ca. 1 atm ethylene at 80 °C, the Cr^{IV} species proved to be inactive for polymerization, consistent with reports that CO reduction temperatures >300 °C are required to generate an active catalyst.[23]

Reduction of Cr^{IV} to Cr^{II}. As the reduction temperature increases further, the UV−vis spectrum remains constant until the temperature reaches 350 °C, when additional changes occur in the spectrum. Over the course of 12 h at 350 °C, the color of the monolith turned from green to blue (Scheme 1b,c). In the UV−vis spectrum, the peak at 465 nm disappeared, whereas the intense, broad peak at 720 nm shifted to 770 nm (Figure 2b). The evolution of the spectra over time shows behavior that is approximately isosbestic, indicating that the second reduction process also occurs very cleanly. The new Cr product is also quite different in its reactivity: when dosed with ca. 1 atm ethylene at 80 °C, the formation of polyethylene was observed by Raman spectroscopy.

High-Frequency/High-Field EPR Spectroscopy. It is generally accepted by Phillips catalyst researchers that Cr^{II} is the final oxidation state attained upon CO reduction of the Phillips precatalyst at $T > 300$ °C.[2] This conclusion was initially based on titration with MnO_4^- and on magnetic susceptibility measurements. The latter gave $\mu_{eff} > 4.8\ \mu_B$ for the reduced catalyst, consistent with high-spin d^4 ions.[9,10,27,28] Subsequent studies employing UV−vis spectroscopy provided additional support for this conclusion.[7] However, direct observation of the Cr^{II} sites has proven elusive, in large part due to their extreme O_2 sensitivity, although XANES evidence for this oxidation state has been reported for heterogeneous materials with high Cr loadings.[29] Electron paramagnetic resonance (EPR) spectroscopy, which is both highly sensitive to and diagnostic of paramagnetic ions, has rarely been used to characterize Cr^{II} compounds since they lack an observable spectrum in the commonly available X- and Q-bands. Their detection, however, is possible by high-frequency/high-field EPR (HFEPR).[30,31]

A Cr^{VI}/SiO_2 xerogel (3.0 mol % Cr) was reduced under CO to its spectroscopically determined end point at 350 °C and then transferred under scrupulously anaerobic conditions to a quartz ampule and sealed. The complete HFEPR spectrum at 106 GHz is shown in Figure S3; Figure 4 (blue) shows the

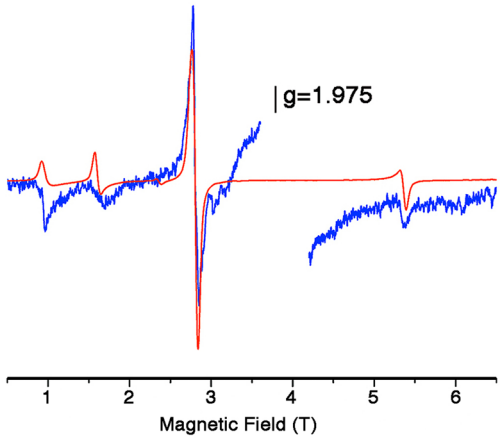

Figure 4. HFEPR spectrum (blue) of the Cr^{II} site generated by reduction of Cr^{VI}/SiO_2 (3.0 mol % Cr) with CO at 350 °C, recorded at 105.6 GHz and 10 K; as well as the simulation of a Cr^{II} powder pattern (red), created using the following spin Hamiltonian parameters: $S = 2$, $D = -2.06\ cm^{-1}$, $E = 0$, $g_{iso} = 1.99$. The signal with a maximum at 3.82 T ($g = 1.975$), arising due to minor Cr^{III} and Cr^V impurities, has been removed. The full spectrum is shown in Figure S3.

same spectrum, but with the high-amplitude signal at $g = 1.975$ (3.82 T) removed (see below). Four features are located far from the $g \sim 2$ spectral region, at fields ranging from 1.0 to 5.5 T. Their presence signifies a non-Kramers (integer spin number) species with a sizable zero-field splitting. Indeed, simulation of a quintet ($S = 2$) spin-state spectrum assuming a true powder distribution reproduces the positions of the features very well (Figure 4, red). Simulation of spectra recorded at 212 and 317 GHz using the same spin Hamiltonian parameters resulted in equally good agreement with experiments (simulation of the 317 GHz spectrum is shown in Figure S4). This observation leaves little doubt that the species responsible for the resonances outside the $g \sim 2$ region is indeed Cr^{II} (for more details, see the Supporting Information). It represents one of the few direct observations of Cr^{II} as the ultimate product of CO reduction, Scheme 1c.

The features at $g = 1.975$ that were removed from Figure 4 likely originate from a superposition of two Kramers forms of Cr (i.e., with half-integer spin numbers): Cr^V ($3d^1$) and Cr^{III} ($3d^3$). Cr^V is a known trace impurity in sol−gel-derived Cr/SiO_2 materials, whereas Cr^{III} is an established minor byproduct of Cr^{VI} reduction in the Phillips catalyst.[27,32] Their large amplitude in the HFEPR spectrum may convey the impression that these resonances represent dominant species. However, this is not the case, for the following reasons. First, Cr^V has no zero-field splitting (zfs), and Cr^{III} is known to have much smaller zfs than Cr^{II}. Consequently, their EPR absorptions converge in a narrow field range around g ∼ 1.98, with correspondingly augmented amplitude. Second, non-Kramers ions typically show much more efficient relaxation than Kramers species, resulting in a significantly weaker EPR

DOI: 10.1021/acscatal.5b00927
ACS Catal. 2015, 5, 5574−5583

response. It is well-known that Kramers ions such as Cr^{III}, Mn^{II}, and V^{IV} produce high-amplitude HFEPR resonances that dominate the spectrum even when present only as trace impurities in complexes of the non-Kramers analogues Cr^{II}, Mn^{III}, and V^{III}, respectively.[31,33,34]

Structures of the Cr sites in Cr/SiO_2. While XANES and EPR spectroscopies are appropriate for determining the oxidation states of Cr as it is progressively reduced to the catalyst precursor, they do not directly address the structures of the Cr sites in each oxidation state, or their uniformity. Recently, we addressed this in an EXAFS study of fully reduced Cr^{II}/SiO_2,[35] concluding that two structures are likely present in a ratio that depends on the catalyst calcination temperature. Both involve Cr^{II} embedded in a six-membered chromasiloxane ring, but with different numbers of additional bonds to Cr from Si−O−Si bridges (Scheme 2). The dominant species, based on the XAFS analysis, is three-coordinate **4**, posited as having a trigonal pyramidal geometry. It was proposed to be the more active site in initiating polymerization, based on the change in its relative abundance as the calcination temperature, and catalytic activity, increases. The less abundant, four-coordinate **3**, suggested to be square pyramidal, was postulated to be less reactive.

Scheme 2. Proposed Structures for Two Chromate Sites (1, 2), Each Embedded in Six-Membered Chromasiloxane Rings (blue) on Highly Dehydroxylated Amorphous Silica; and the Resulting Cr^{II} Sites (3, 4) Formed upon CO Reduction,[35,36] as well as the Corresponding Carbonyl Complexes (5, 6)[a]

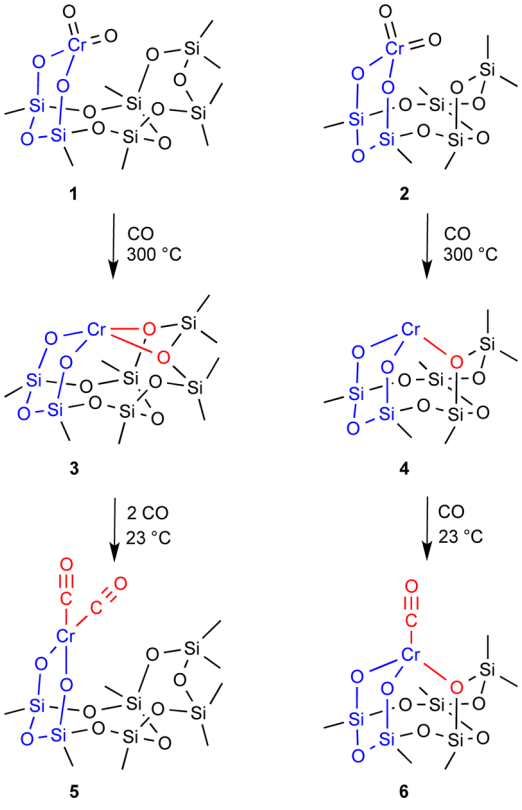

[a]Additional siloxane and carbonyl ligands are shown in red. Adapted from and reprinted with permission from ref 35. Copyright 2012 Elsevier.

Electronic spectra of Cr^{II} species with coordination numbers of four or fewer are extremely rare, due to the high reactivity of these compounds.[37] Using the sol−gel matrix, we obtained high quality transmission UV−vis spectra of the Cr^{II} sites, recorded under rigorously anaerobic conditions. Figure 5 shows the spectrum of a Cr^{II}/SiO_2 monolith (0.5 mol % Cr), reduced at 350 °C until no further spectral changes were observed. Two bands are observed in the visible and near IR: a relatively intense band at 770 nm (ε = 2240 M^{-1} cm^{-1}) and a very broad, weak band centered at 1229 nm (ε = 354 M^{-1} cm^{-1}); notably, the magnitudes of the extinction coefficients are consistent with ligand field transitions of low symmetry ions. Similar spectral features for the Cr^{II} were also reported by Budnyk et al., using the same approach of studying the Phillips catalyst with sol−gel materials.[38]

In general, it is problematic to make structural assignments on the basis of electronic spectra, particularly in complex systems containing multiple species and oxidation states. Nevertheless, it is worthwhile to investigate whether the general features of the spectrum are consistent with our expectations for low-coordinate structures of Cr^{II} (e.g., **3** and **4** in Scheme 2). In rigorous tetrahedral symmetry, Cr^{II} has only one spin-allowed ligand field transition, from the $^5T_2$ ground state to the ^5E excited state, and it typically occurs in the near-infrared. For example, $CrCl_4^-$ exhibits a weak, broad peak at 1020 nm assigned to that $^5T_2 \rightarrow {}^5E$ ligand field transition.[37] Moreover, Cr^{II} substituted into the tetrahedral sites of semiconductors such as CdS and ZnTe (which have weaker ligand fields than oxides) show low-intensity, low-energy ligand field bands at 1786 and 1820 nm, respectively.[40,41] In fact, emission from these low energy ligand field states has been investigated extensively for near-infrared laser applications.[42] Thus, the presence of the band at 1229 cm^{-1} in Figure 5 can be viewed as diagnostic of Cr^{II} ions in a low coordination environment.

The assignment of the much more intense, higher-energy transition at 770 nm is less obvious, although Cr^{II}-doped CdS and ZnTe exhibit transitions with similar relative intensities at 800 and 1000 nm, respectively.[40,41] The symmetry of the Cr sites in Cr^{II}/SiO_2 is lower than tetrahedral, thus the appearance of the second transition in Figure 5 is consistent with this reduction in symmetry. Structure **4** in Scheme 2, which was suggested to be the dominant structure present in the reduced Phillips catalyst, with approximate C_{3v} symmetry, is closer to pseudotetrahedral than structure **3**.[35] The symmetry reduction splits the triply degenerate $^5T_2$ ground state into $^5A_1$ and ^5E states (the higher ^5E state is unaltered), giving rise to two $^5A_1 \rightarrow {}^5E$ spin-allowed transitions. The actual structure of the three-coordinate site will likely have even lower symmetry, as suggested by the unequal bond lengths found by EXAFS,[35] further removing degeneracy. Using multiconfigurational second-order perturbation theory (CASPT2), Espelid and Børve calculated the electronic spectrum for a Cr^{II} site attached to the surface by two Si−O−Cr linkages, $(\equiv SiO)_2Cr^{II}$, as a model for the Phillips Cr^{II} site.[43] Its C_{2v} symmetry results in a complete removal of the degeneracy of the T and E states found in T_d symmetry. Their calculations predict a $^5B_1$ ground state with two fully allowed transitions at 1191 and 813 nm, corresponding to the $1^5B_1 \rightarrow 1^5A_1$ and the $1^5B_1 \rightarrow 2^5A_1$ ligand field transitions, respectively. These band positions agree quite well with the observed spectrum of Cr^{II}/SiO_2 in Figure 5. In contrast, four-coordinate Cr^{II} (Scheme 2, structure **3**), derived from octahedral symmetry by tetragonal distortion to square-planar, should have three spin-allowed ligand field bands. Cr^{II} species in tetragonally distorted octahedral fields are well-

DOI: 10.1021/acscatal.5b00927
ACS Catal. 2015, 5, 5574−5583

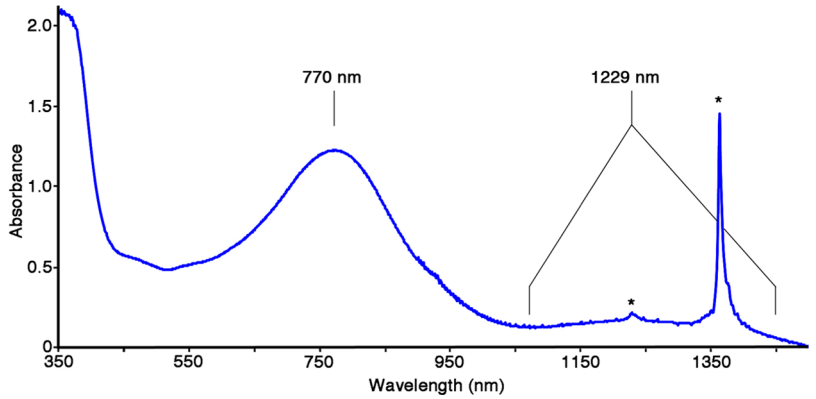

Figure 5. UV−vis spectrum of the Cr^{II} site obtained by reduction of a Cr^{VI}/SiO_2 xerogel (0.5 mol % Cr) with flowing CO at ambient pressure and 350 °C. (Note: sharp features marked with * are overtone and combination bands associated with residual surface silanols.)[39]

known, and their lowest energy transitions are typically much higher in energy than those observed for four-coordinate species.[37] Of course, species such as **3** could contribute to the higher energy regions of the spectrum, as could the minor Cr^{III} sites formed during CO reduction. However, the spectrum and, in particular, the broad low energy transition at 1229 cm^{-1}, are consistent with low symmetry Cr^{II}.

The transparency of the Cr-SiO_2 sol−gel monoliths in the visible region also greatly facilitates the collection of Raman spectra, which can provide complementary structural information about the Cr sites as a function of the degree of reduction. Figure 6 shows Raman spectra in the region below 1300 cm^{-1}, where the Cr−O vibrations are expected.[44] The vibrational spectrum of Cr^{VI}/SiO_2, shown in Figure 6a, has already been assigned in some detail.[5,44] The intense band at 982 cm^{-1} is typically attributed to totally symmetric, predominantly terminal, CrO_2 stretching. The origin of the weaker band at 997 cm^{-1} is complex and includes contributions from antisymmetric CrO_2 stretching. The spectrum in Figure 6b was acquired immediately following CO reduction for 1 h at 230 °C to generate the Cr^{IV} site. It shows a very intense, sharp band at 988 cm^{-1} (fwhm 8 cm^{-1}) with a shoulder on the high energy side (ca. 1000 cm^{-1}). As indicated in Scheme 1b, the first reduction by CO is proposed to remove one of the two terminal oxo ligands from the grafted chromate ester. Since the 988 cm^{-1} band occurs in the spectral region associated with the terminal Cr═O stretches of the bis(oxo)Cr^{VI} site, and since the band is similarly sharp and intense, we tentatively assign it to a mode dominated by Cr═O stretching of mono(oxo)Cr^{IV} (i.e., chromyl). Consistent with this assignment, the band is strongly polarized, indicating that it is a symmetric stretch. It is unlikely, however, that the Cr^{IV} site is as coordinately unsaturated as depicted in Scheme 1b. It likely coordinates to the silica through one or two additional siloxane ligands (resulting in nominal C_{3v} or C_{4v} site symmetry). In fact, the Raman spectrum in Figure 6b is very similar to that of a nominally C_{3v}-symmetry silica-supported vanadyl, $(\equiv SiO)_3V{=}O$.[45,46] Finally, we note that the Raman spectra of the Cr^{IV} material was collected using 633 nm excitation, which yielded the highest quality spectrum. However, since excitation at this wavelength impinges on the electronic absorption bands, resonant enhancement of the metal oxo bands can occur.

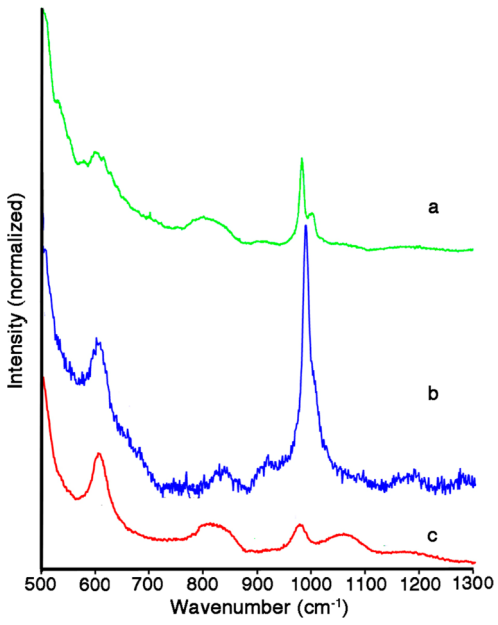

Figure 6. Raman spectra of Cr/SiO_2 (1.0 mol % Cr), after (a) calcination at 500 °C; (b) reduction by CO at 230 °C; and (c) reduction by CO at 350 °C, followed by evacuation to remove CO. Spectrum (a) was collected using 785 nm excitation to avoid luminescence from the Cr^{VI} site, while spectra (b) and (c) were collected using 633 nm excitation. Intensities of the intrinsic silica features below ca. 900 cm^{-1} are normalized across the spectra.

The Raman spectrum after CO reduction to Cr^{II} at 350 °C is shown Figure 6c. Consistent with removal of the last terminal oxo ligand (Scheme 1c), the sharp band at 988 cm^{-1} is absent. The only band clearly attributable to the Cr^{II} site is a weak band at 977 cm^{-1} (fwhm 25 cm^{-1}). All other bands are modes intrinsic to SiO_2, although the spectral region below ∼1100 cm^{-1} is congested and likely contains contributions from Si−O−Si and Si−O−Cr modes.[47,48]

Adsorbed CO as a Probe of the Cr^{II} Sites. After CO reduction at 350 °C, the most prominent feature in the Raman spectrum is a sharp, very intense band at 2183 cm^{-1}, Figure 7a. This band, as well as three significantly weaker bands at 2155, 2137, and 2119 cm^{-1}, have been observed previously by IR spectroscopy and represent stretching modes associated with CO coordinated to the Cr^{II} sites.[3,11,35] Evacuating the system (10^{-4} Torr) overnight at room temperature caused the low frequency CO modes to disappear, leaving only the attenuated high frequency band (Figure 7b). Heating under vacuum for 2 h at 250 °C (Figure 7c) resulted in almost complete removal of

DOI: 10.1021/acscatal.5b00927
ACS Catal. 2015, 5, 5574−5583

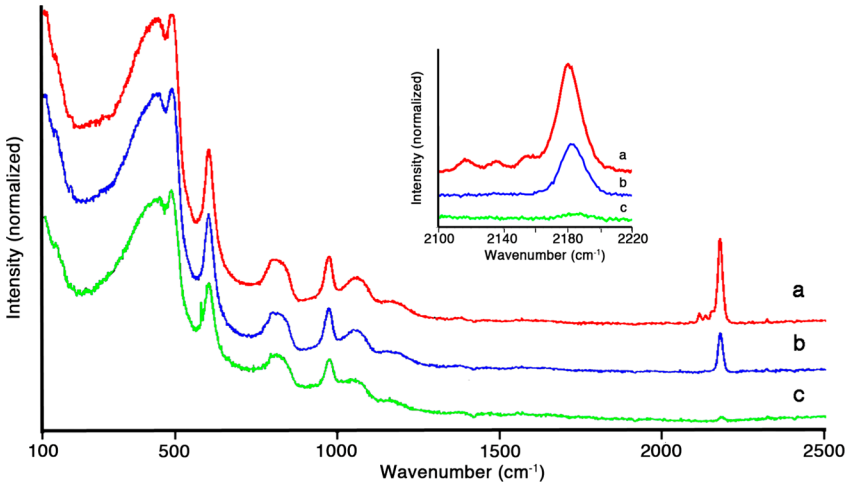

Figure 7. Raman spectra of Cr/SiO_2 (1.0 mol % Cr): (a) immediately after reduction with CO at 350 °C for 4 h, (b) after subsequent evacuation overnight (10^{-4} Torr), and (c) after evacuation for 2 h (10^{-4} Torr) at 250 °C. Spectra are normalized to the intensity of the low frequency silica modes that are invariant.

CO, with only a weak remnant of the band at 2183 cm^{-1} still visible. Once the CO is removed, re-exposure of Cr^{II}/SiO_2 to CO at room temperature regenerates the initial spectrum, showing all four bands at the same relative intensities. Excitation into the absorption bands of the Cr^{II} ions makes resonant enhancement of the carbonyl stretches possible. The modes that are enhanced depend on their symmetry, as well as that of the excited state being pumped. An inherently low symmetry system such as this one will likely experience enhancement of the totally symmetric vibrational modes (i.e., A-term enhancement). However, resonant enhancement of carbonyl stretches typically occurs through excitation into LMCT bands involving the carbonyl, which is not the case here.[49−51] Regardless, we refrain from drawing quantitative conclusions from the relative intensities of the bands.

Carbonyl ligands coordinated to the Cr^{II} sites of the Phillips catalyst have been studied extensively by IR, with the goal of distinguishing Cr^{II} sites having different coordination geometries. In earlier studies of the Phillips catalyst, made through traditional wet impregnation of silica with Cr^{III} compounds, three IR bands at 2191, 2184, and 2179 cm^{-1} were observed at CO pressures roughly corresponding to our experimental conditions (ca. 1 atm CO). These bands were assigned to monocarbonyl (2191 cm^{-1}) and dicarbonyl (2184 and 2179 cm^{-1}) sites.[3] In a study of a model Phillips catalyst made by anhydrous grafting of CrO_2Cl_2 onto silica, three carbonyl bands were also observed at similar frequencies: 2191, 2186, and 2179 cm^{-1}.[35] Based on their correlated changes in intensity as CO was progressively removed from the catalyst, the bands at 2191 and 2179 cm^{-1} were determined to belong to the same site and were assigned to the symmetric and antisymmetric modes of a dicarbonyl species, whereas the band at 2186 cm^{-1}, whose intensity is independent of the other two, was assigned to the stretching of a monocarbonyl species.

The position of the most intense band at 2183 cm^{-1} agrees well with that of the band assigned to the monocarbonyl site by Zhong et al.[35] In comparison to IR spectra of comparable materials made by wet impregnation or grafting onto silica, the observable bands are spread out over a somewhat larger spectral window, from ca. 2110 to 2200 cm^{-1}. Although we cannot completely rule out the possibility that we are observing carbonyl species not detected in previous IR studies, this seems unlikely given the much lower inherent sensitivity of Raman experiments. Because it is known that metal carbonyl vibrations both broaden and shift in energy due to interactions with metal oxide surfaces,[52,53] the spreading of the mono- and dicarbonyl stretching frequencies over a wider spectral window likely arises from interactions of the carbonyl groups with walls of the silica xerogel network instead. Although the sol−gel matrix is mesoporous, the pore size distribution is broad, with a significant microporous region. Consequently, Cr sites incorporated into the matrix by co-condensation may experience microenvironments that allow interactions of the carbonyl ligands with the matrix surrounding them.

Raman spectra for CO-reduced Cr^{II}/SiO_2, collected under both parallel and perpendicular polarization conditions, are shown in Figure 8. The intense band at 2183 cm^{-1} is strongly polarized, as are the two weaker bands at 2155 and 2137 cm^{-1}, indicating that they are all totally symmetric modes. Only one transition, the lowest energy mode at 2119 cm^{-1}, is nonpolarized. It can therefore be assigned with certainty to the antisymmetric stretch of a dicarbonyl species. With this assignment, two of the totally symmetric bands are assignable to the symmetric modes of mono- and dicarbonyl species, while the assignment of the third is unclear.

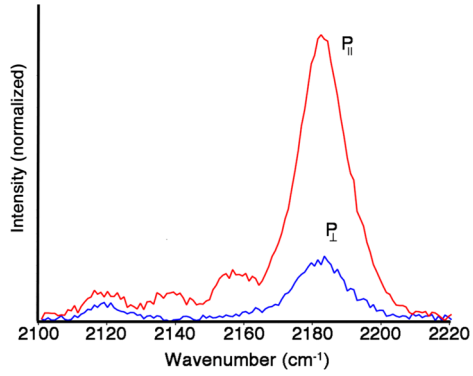

Figure 8. Parallel- and perpendicularly polarized Raman spectra of the carbonyl stretching region, for Cr^{II}/SiO_2 (1.0 mol % Cr) prepared by reduction with CO at 350 °C for 4 h.

DOI: 10.1021/acscatal.5b00927
ACS Catal. 2015, 5, 5574−5583

To aid in assigning the totally symmetric bands, a DFT calculation was carried out on an optimized dicarbonyl site, based on structure **5** in Scheme 2 (see Supporting Information). The unscaled values of the predicted frequencies for the antisymmetric and symmetric carbonyl stretches are 2183 and 2212 cm^{-1}, respectively (Table 1). Notably, the antisymmetric mode appears at the lower energy, consistent with its assignment in the experimental spectrum. Because its experimental frequency is known, it was used to obtain a frequency-independent multiplicative scaling factor (0.971).[54] Using this scaling factor, the calculated frequency of the symmetric stretch is 2152 cm^{-1}, in very good agreement with the band observed at 2155 cm^{-1}. The difference between the symmetric and antisymmetric stretches is 36 cm^{-1}, larger than that observed by Zhong et al.[35] However, the energy difference between the symmetric and antisymmetric components depends strongly on the angle between the carbonyls through the cosine dependence of the off-diagonal terms that couple them in the Wilson FG matrix. Our results indicate that the angle is larger in these xerogel materials than for materials made by grafting CrO_2Cl_2 onto nonporous silica, consistent with interactions imposed by the xerogel pore system.

Table 1. Experimental and Calculated Frequencies for Mono- and Dicarbonyl Cr^{II} Sites

site	assignment	experimental (cm^{-1})	calculated (cm^{-1})
$Cr(^{12}CO)_2$	ν_s	2155	2152[a]
	ν_a	2119	2119[a]
$Cr(^{12}CO)$	ν_s	2183	2183[b]
$Cr(^{13}CO)$	ν_s	2137	2131[b]

[a]Scaled by a factor of 0.971. [b]Scaled by a factor of 0.988, which brings the calculated band into agreement with the ^{12}CO symmetric stretch so the frequency of the ^{13}CO band could be predicted.

The totally symmetric stretch at 2183 cm^{-1} is therefore assigned with confidence to a monocarbonyl site, by comparison to the reported IR frequency for that site at 2186 cm^{-1}.[35] Our DFT calculations for structure **6** predict the unscaled frequency of this band to be 2210 cm^{-1}, within 1.2% of the observed value and well within the accepted range for DFT calculations (see Supporting Information). Thus, the only peak that remains to be assigned is the weak, symmetric band at 2137 cm^{-1}. It may be, at least in part, the ^{13}C contribution of the intense monocarbonyl mode. The DFT-calculated frequency for the stretching of $Cr(^{13}CO)$ is 52 cm^{-1} lower than the $Cr(^{12}CO)$ mode, or 2131 cm^{-1}, in very good agreement with the frequency of the unassigned band, Table 1. The ratio of integrated intensities for the $Cr(^{13}CO)/Cr(^{12}CO)$ modes is approximately 6%, which is higher than the natural abundance of ^{13}C (ca. 1%). Thus, we cannot rule out a contribution from another monocarbonyl site, possibly derived from structure **5** through loss of a carbonyl. One final point worth noting is that coordination of CO appears to result in little or no perturbation of the metal-oxide region of the Raman spectrum. The lack of coupling is consistent with weak Cr-CO bonding, as expected for Cr^{III} with its relatively poor π-back-donation properties.

Reaction of Cr^{II} Sites with Ethylene, Resulting in Oxidation to Cr^{III}. While reduction of Cr^{VI} to Cr^{II} is necessary to generate the precatalyst, the organoCr active sites ultimately arise from the reaction of Cr^{II} with ethylene.[2,9] To prepare and isolate these sites, a Cr^{VI}/SiO_2 monolith was first treated at 350 °C under flowing CO, while the progress of the reduction was monitored by UV−vis spectroscopy. Reduction to Cr^{II} was judged to be complete when no further spectral changes were observed. The monolith was then flushed with Ar to remove all CO, both infused and coordinated. The full spectrum of the Cr^{II} site prior to reaction with ethylene is shown in Figure 9a as spectrum 1. After reduction, the temperature was reduced to 80 °C, and the sample was "titrated" with highly dilute aliquots of ethylene; after each injection, a UV−vis spectrum was recorded (Figure 9b).

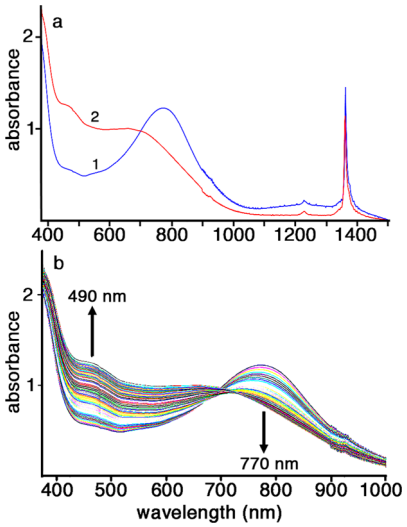

Figure 9. UV−vis spectra of (a) the Cr^{II} precatalyst, before its reaction with ethylene (1) and after its complete reaction with ethylene (2); and (b) spectroscopic changes recorded for a 0.5 mol % Cr/SiO_2 xerogel initially reduced with CO at 350 °C, then titrated with aliquots of ethylene at 80 °C. (Note: the sharp features at ca. 1375 and 1230 nm are overtone and combination bands associated with silanol fundamentals.)[39]

The spectrum changes slowly but dramatically over the course of the titration, with the peak at 770 nm disappearing and a new peak at 490 nm emerging. Consistent with the spectral changes, the material changes from pale blue to dark green during this process (Scheme 1c,d). The reaction appears to proceed cleanly, albeit with deviation from a true isosbestic point at ca. 700 nm. The final spectrum after titration, when no further spectral changes are observed, is shown in Figure 9a as spectrum 2. Three independent samples were treated in this way until no further spectral changes were observed. Elemental analysis of these materials revealed the presence of carbon, consistent with the product being an organoCr species. (Control samples of Cr/SiO_2 xerogels showed, at best, trace amounts of carbon both before and after CO reduction.) Quantitative analysis yielded an average C/Cr ratio of (1.9 ± 0.2) (see Supporting Information), suggesting that at the end point of the titration, when no further changes are observed in the UV−vis spectrum, the material has taken up, on average, one ethylene per Cr site.

The oxidation state of the ethylene-titrated sample was determined from Cr $L_{2,3}$-edge XANES, by comparison to the binary oxides of Cr as reference standards (Figure S7). The XANES is consistent with Cr^{III}, Figure 10, with no evidence for Cr^{II} or, as has been postulated for the Phillips initiating site, Cr^{IV}.[3]

DOI: 10.1021/acscatal.5b00927
ACS Catal. 2015, 5, 5574−5583

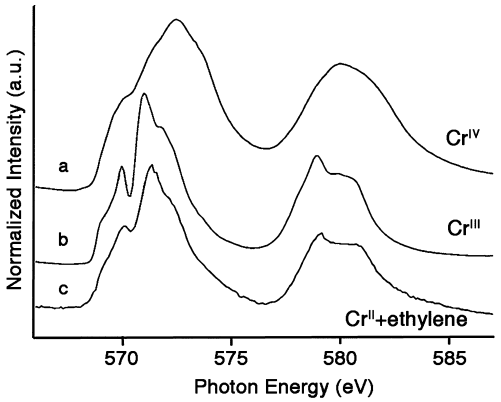

Figure 10. Comparison of the Cr $L_{2,3}$-edge XANES for reference spectra of the bulk binary Cr oxides of (a) Cr^{IV}; and (b) Cr^{III}; as well as (c) the organoCr^{III} site generated by titration of CO-reduced Cr^{II}/SiO_2 with ethylene.

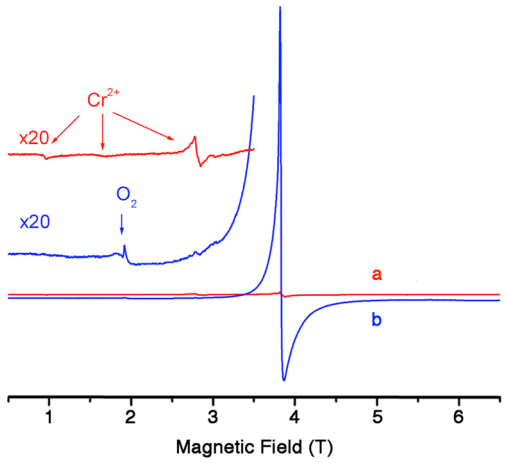

Figure 11. HFEPR spectra of (a) Cr^{II}/SiO_2 (3.0 mol % Cr) resulting from the reduction of Cr^{VI}/SiO_2 with CO at 350 °C (red); and (b) after its titration with ethylene at 80 °C to give the organoCr^{III} sites (blue). Experimental conditions as in Figure 4.

The UV−vis spectrum is consistent with the oxidation state at the end of the ethylene titration being Cr^{III}. The final spectrum (Figure 9a, spectrum 2) is characterized by two resolved but strongly overlapping bands at 676 nm (1240 M^{-1} cm^{-1}) and 463 nm (1570 M^{-1} cm^{-1}). Notably absent is any intensity above ca. 1100 nm, which would be associated with persistent Cr^{II}. As described above, the Cr^{II} sites in the precatalyst exist in a weak ligand-field environment and most have low coordination numbers (3 or 4). Upon reaction with ethylene, the resulting Cr^{III} sites will likely have higher coordination numbers and, due to the presence of the organic ligand, lower symmetry. Spectroscopic characterization of Cr^{III} ions substituted into the octahedral sites of oxide matrices reveals two spin-allowed ligand field bands, $^4A_{2g} \rightarrow {}^4T_{2g}$ and $^4A_{2g} \rightarrow {}^4T_{1g}$. For example, they are observed at 580 and 430 nm in Cr-doped $MgGa_2O_4$, and at 580 and 410 nm in Cr-doped $KZnClSO_4$.[55,56] Cr^{III} in tetrahedral sites also shows two ligand field transitions, both $^4T_1 \rightarrow {}^4T_1$, and both observed at much longer wavelengths. For example, bands at 765 and 1490 nm were reported for Cr^{III} substituted into a lithium−gallium spinel.[57] The transitions observed for the Phillips active sites are clearly more consistent with Cr^{III} in an octahedral ligand field. However, we do not wish to imply that the site is rigorously octahedral. Instead, it likely has a coordination number higher than four. Notably, the magnitude of the extinction coefficients are consistent with Laporte-allowed transitions, which suggests a symmetry lower than octahedral.[37] It is also significant that transformation of (nominally) distorted tetrahedral Cr^{II} to (nominally) distorted octahedral Cr^{III} would result in a large gain in ligand field stabilization energy, which would help to drive the one-electron oxidation process.

Further evidence for the oxidation state change upon reaction of Cr^{II}/SiO_2 with ethylene is found in the HFEPR spectrum. Resonances associated with Cr^{II} disappear from the spectrum upon exposure to the olefin (Figure 11). Concomitant with the loss of the non-Kramers Cr^{II} resonances, the intensity of the transitions belonging to the Kramers spin at ca. $g = 2$ (3.77 T) increases dramatically, consistent with oxidation of Cr^{II} to Cr^{III}. Notably, no signals are detected for Cr^{IV} which, being a non-Kramers ion, like Cr^{II}, should therefore have resonances that are well separated from the Kramers region of the spectrum.

Relevant to a recent claim that Cr^{II} in the Phillips catalyst is not active toward ethylene,[58] the results presented here clearly and unambiguously demonstrate that reduction of the Cr^{VI} sites leads, ultimately, to the generation of Cr^{II}, and that when this oxidation state is attained, the resulting fully reduced sites are capable of reacting with ethylene. Significantly, exposure to ethylene leads to facile oxidation of Cr^{II} to Cr^{III}, as shown by the complete disappearance of the characteristic Cr^{II} ($^5T_2 \rightarrow {}^5E$) ligand field transition at 1229 nm in the UV−vis spectrum, the loss of Cr^{II} resonances in the HFEPR spectrum and the concomitant appearance of resonances associated with Cr^{III} in the Kramers region of the EPR spectrum, as well as the characteristic XANES of Cr^{III}. The measured uptake of carbon during this final redox process shows the reaction to be essentially quantitative. This suggests that the organoCr site is a Cr^{III} site and is not generated from existing Cr^{III} impurities (although ions in that oxidation state exist as a minor byproduct of the Cr^{VI} reduction) but in a reaction involving the Cr^{II} precatalyst.

The suggestion that Cr^{II} is not a necessary participant in Phillips catalyst activation was predicated on the observation that no polymerization was observed over a model catalyst prepared by depositing a molecular Cr^{II} complex onto a silica surface.[58] In our view, the lack of polymerization activity by this particular catalyst under the reported conditions does not necessarily reflect on the mechanism of Phillips catalyst activation. Phillips practitioners know that the catalyst is extraordinarily sensitive to even trace amounts of adventitious oxygen and water, a property attributed to the extreme reactivity of the Cr^{II} sites. Commercial Phillips-based polymerization requires rigorously clean conditions, as described by McDaniel.[2] Moreover, it is important to note that the model catalyst differs in a number of ways from the actual Phillips catalyst, which calls into question whether any meaningful conclusions can be drawn from its activity or lack thereof. In particular, the catalyst is composed of oxo-bridged Cr^{II} *dimers*, while the Phillips catalyst, like many other supported metal oxide catalysts, shows its highest activity at submonolayer coverages. This is generally attributed to the high reactivity of isolated Cr sites, and reactivity declines when oligomeric Cr is present. The EXAFS of the highly active Cr^{II} precatalyst sites reported by Zhong et al. indicated only monomeric Cr^{II} sites, in

DOI: 10.1021/acscatal.5b00927
ACS Catal. 2015, 5, 5574−5583

differing coordination environments.[35] Thus, the inability of a model Cr^{II} catalyst to polymerize ethylene may merely reflect the poor reactivity of dimeric and oligomeric Cr^{II}. Finally, the modest polymerization activity of a related model supported Cr^{III} complex is not unprecedented in prior literature. The phenomenon has been discussed by McDaniel in his review of the Phillips process,[2] which notes that, while superlative results have often been claimed for polymerization by Cr^{III}, commercial reactors have never been able to confirm anything but minimal activity. Our own recent computational study of the proposed nonredox-based initiation by ethylene deprotonation revealed it to be implausible for *both* Cr^{II} and Cr^{III}.[59]

In summary, our results show that the generation of the Phillips catalyst active sites occurs through a multistep redox process which converts the supported Cr^{VI} sites to Cr^{II}. This finding is consistent with many other prior studies of the Phillips system. Using CO as the reductant, the Cr^{IV} sites were obtained as intermediates. However, they retain a terminal oxo ligand and are unreactive toward ethylene. Distinct from previous studies, we find that the Cr^{II} sites are oxidized to organoCr^{III} sites in a stoichiometric reaction with ethylene. The resulting material polymerizes ethylene, suggesting that these organoCr^{III} species are the initiating sites.

EXPERIMENTAL METHODS

Fabrication of Cr-SiO_2 Xerogels. Transparent, porous silica xerogels containing between 0.5 and 3.0 mol % Cr were made by co-condensation of tetramethylorthosilicate (TMOS) with CrO_3 in an aqueous ethanol solution, following published procedures.[5,16] The solutions were allowed to gel, aged at room temperature over a period of 3−4 months, then slowly dried in air at 100 °C and calcined at 500 °C. This resulted in transparent yellow-orange monoliths (depending on the Cr concentration), containing Cr^{VI} sites well dispersed throughout the silica matrix.

CO Reduction and Ethylene Titration of Cr-SiO_2 Xerogels. In situ monitoring of reduction of the Cr/SiO_2 materials was carried out in a closed, high-temperature/high-pressure UV−vis cell equipped with sapphire windows. In a typical experiment, a Cr^{VI}/SiO_2 xerogel monolith (1.5 × 0.5 × 0.5 mm) was mounted in the cell and calcined in flowing O_2 at 230 °C for approximately 2 h. Reduction was carried out under flowing CO isothermally at either 230 or 350 °C while monitoring the changes in the UV−vis spectrum. Reduction was considered complete when the spectrum ceased to change. Oxidation by ethylene was monitored by delivering small aliquots of ethylene to the Cr^{II}/SiO_2 monolith at 80 °C, while monitoring the spectral changes.

X-ray Absorption Near-Edge Spectroscopy. Hard X-ray absorption near-edge spectroscopy (XANES) data at the Cr *K*-edge was acquired on beamline BL2−3 (Bend) at the Stanford Synchrotron Radiation Laboratory (SSRL). Soft XANES data were acquired at undulator beamline 8.0.1 at the Advanced Light Source (ALS) of Lawrence Berkeley National Laboratory. Spectra of binary oxide standards were recorded for samples pressed as powders onto carbon tape.

HFEPR Spectroscopy. HFEPR experiments were performed at the National High Magnetic Field Laboratory Laboratory, using a home-built instrument described previously.[60] HFEPR spectra were acquired for Cr^{II}/SiO_2 and Cr^{III}/SiO_2 (3.0 mol % Cr), packed into sealed quartz ampules under rigorously anaerobic and anhydrous conditions, at three frequencies (ca. 106, 212, and 317 GHz).

Raman Spectroscopy. Raman spectra were collected on Cr/SiO_2 xerogel monoliths (1.5 × 0.5 × 0.5 mm^3, 1.0 mol % Cr). Samples were placed in a quartz cell equipped with a cylindrical reaction container for in situ high temperature experiments, attached to a side arm equipped with a spectroscopic cell. Raman spectra were obtained using a micro-Raman spectrograph (JY Horiba LabRam HR800), with excitation at 633 nm (HeNe laser) or 785 nm (infrared diode laser).

COMPUTATIONAL METHODS

Density Functional Calculations. Structural models used in the computational analysis of vibrational frequencies were built and optimized using Spartan'10, v.1.1.0 and Spartan'14, v.1.1.4 (Wave function, Inc. Irvine, CA; www.wavefun.com) running on a MacBook Pro. Chromasiloxane model structures were built to correspond to surface models **3** and **4** in Scheme 2, as suggested by EXAFS.[35]

ASSOCIATED CONTENT

Supporting Information

The Supporting Information is available free of charge on the ACS Publications website at DOI: 10.1021/acscatal.5b00927.

Materials, methods, and experimental details of each step in the reaction sequence, as well as product characterization and Cartesian coordinates of calculated structures (PDF)

Structural models as sdf files (ZIP)

AUTHOR INFORMATION

Corresponding Authors

*E-mail: stiegman@chem.fsu.edu.

*E-mail: sscott@engineering.ucsb.edu.

Notes

The authors declare no competing financial interest.

ACKNOWLEDGMENTS

This work was carried out with funding provided by the Catalysis Science Initiative of the U.S. Department of Energy, Basic Energy Sciences (DE-FG02-03ER15467). The work was also supported by the National High Magnetic Field Laboratory, which is funded by NSF (Cooperative Agreement DMR 1157490), the State of Florida, and the U.S. Department of Energy. Use of the Stanford Synchrotron Radiation Lightsource, SLAC National Accelerator Laboratory, is supported by the U.S. Department of Energy, Office of Science, Office of Basic Energy Sciences under Contract No. DE-AC02-76SF00515. The Advanced Light Source is supported by the Director, Office of Science, Office of Basic Energy Sciences, of the U.S. Department of Energy under Contract No. DE-AC02-05CH11231.

REFERENCES

(1) Hogan, J. P.; Banks, R. L. Polymers and production thereof. U.S. Patent 2825721, March 4, 1958.

(2) McDaniel, M. P. In *Advances in Catalysis*; Gates, B. C., Knozinger, H., Eds.; Elsevier: Amsterdam, 2010; Vol. *53*, pp 123−606.

(3) Groppo, E.; Lamberti, C.; Bordiga, S.; Spoto, G.; Zecchina, A. *Chem. Rev.* **2005**, *105*, 115−183.

(4) McDaniel, M. P. In *Handbook of Heterogeneous Catalysis*, 2nd ed.; Ertl, G., Knozinger, H., Schuth, F., Weitkamp, J., Eds.; Wiley-VCH: Weinheim, 2008; pp 3733−3792.

DOI: 10.1021/acscatal.5b00927
ACS Catal. 2015, 5, 5574−5583

(5) Moisii, C.; Deguns, E. W.; Lita, A.; Callahan, S. D.; van de Burgt, L. J.; Magana, D.; Stiegman, A. E. *Chem. Mater.* **2006**, *18*, 3965−3975.
(6) Weckhuysen, B. M.; Wachs, I. E.; Schoonheydt, R. A. *Chem. Rev.* **1996**, *96*, 3327−3350.
(7) Weckhuysen, B. M.; Schoonheydt, R. A.; Jehng, J. M.; Wachs, I. E.; Cho, S. J.; Ryoo, R.; Kijlstra, S.; Poels, E. *J. Chem. Soc., Faraday Trans.* **1995**, *91*, 3245−3253.
(8) Guesmi, H.; Tielens, F. *J. Phys. Chem. C* **2012**, *116*, 994−1001.
(9) Krauss, H. L.; Stach, H. *Inorg. Nucl. Chem. Lett.* **1968**, *4*, 393−397.
(10) Krauss, H. L.; Stach, H. *Z. Anorg. Allg. Chem.* **1969**, *366*, 280−290.
(11) Ghiotti, G.; Garrone, E.; Zecchina, A. *J. Mol. Catal.* **1991**, *65*, 73−83.
(12) Krauss, H. L.; Hagen, K.; Hums, E. *J. Mol. Catal.* **1985**, *28*, 233−238.
(13) Delley, M. F.; Conley, M. P.; Copéret, C. *Catal. Lett.* **2014**, *144*, 805−808.
(14) Delley, M. F.; Núñez-Zarur, F.; Conley, M. P.; Comas-Vives, A.; Siddiqi, G.; Norsic, S. b.; Monteil, V.; Safonova, O. V.; Copéret, C. *Proc. Natl. Acad. Sci. U. S. A.* **2014**, *111*, 11624−11629.
(15) Peters, B.; Scott, S. L.; Fong, A.; Wang, Y.; Stiegman, A. E. *Proc. Natl. Acad. Sci. U.S.A.* **2015**, *112*, E4162−E4163.
(16) Stiegman, A. E.; Eckert, H.; Plett, G.; Kim, S. S.; Anderson, M.; Yavrouian, A. *Chem. Mater.* **1993**, *5*, 1591−1594.
(17) Curran, M. D.; Poore, D. D.; Stiegman, A. E. *Chem. Mater.* **1998**, *10*, 3156−3166.
(18) Soult, A. S.; Carter, D. F.; Schreiber, H. D.; van de Burgt, L. J.; Stiegman, A. E. *J. Phys. Chem. B* **2002**, *106*, 9266−9273.
(19) Soult, A. S.; Poore, D. D.; Mayo, E. I.; Stiegman, A. E. *J. Phys. Chem. B* **2001**, *105*, 2687−2693.
(20) Tran, K.; Hanninglee, M. A.; Biswas, A.; Stiegman, A. E.; Scott, G. W. *J. Am. Chem. Soc.* **1995**, *117*, 2618−2626.
(21) Tran, K.; Stiegman, A. E.; Scott, G. W. *Inorg. Chim. Acta* **1996**, *243*, 185−191.
(22) Brown, C.; Achey, R.; Fu, R. Q.; Gedris, T.; Stiegman, A. E. *J. Am. Chem. Soc.* **2005**, *127*, 11590−11591.
(23) Welch, M. B.; McDaniel, M. P. *J. Catal.* **1983**, *82*, 110−117.
(24) Weckhuysen, B. M.; Deridder, L. M.; Schoonheydt, R. A. *J. Phys. Chem.* **1993**, *97*, 4756−4763.
(25) Krauss, H. L. *J. Mol. Catal.* **1988**, *46*, 97−108.
(26) Krauss, H. L.; Hanke, B. *Z. Anorg. Allg. Chem.* **1985**, *521*, 111−121.
(27) McDaniel, M. P. In *Advances in Catalysis*; Eley, D. D., Pines, H., Weisz, P. B., Eds.; Elsevier: Amsterdam, 1985; Vol. *33*, pp 47−98.
(28) Zecchina, A.; Garrone, E.; Ghiotti, G.; Morterra, C.; Borello, E. *J. Phys. Chem.* **1975**, *79*, 966−972.
(29) Groppo, E.; Prestipino, C.; Cesano, F.; Bonino, F.; Bordiga, S.; Lamberti, C.; Thüne, P. C.; Niemantsverdriet, J. W.; Zecchina, A. *J. Catal.* **2005**, *230*, 98−108.
(30) Dobe, C.; Noble, C.; Carver, G.; Tregenna-Piggott, P. L. W.; McIntyre, G. J.; Barra, A. L.; Neels, A.; Janssen, S.; Juranyi, F. *J. Am. Chem. Soc.* **2004**, *126*, 16639−16652.
(31) Telser, J.; Pardi, L. A.; Krzystek, J.; Brunel, L. C. *Inorg. Chem.* **1998**, *37*, 5769−5775.
(32) Tanaka, K.; Kamiya, K. *J. Mater. Sci. Lett.* **1991**, *10*, 1095−1097.
(33) Harvey, J. D.; Ziegler, C. J.; Telser, J.; Ozarowski, A.; Krzystek, J. *Inorg. Chem.* **2005**, *44*, 4451−4453.
(34) Horton, D. C.; VanDerveer, D.; Krzystek, J.; Telser, J.; Pittman, T.; Crans, D. C.; Holder, A. A. *Inorg. Chim. Acta* **2014**, *420*, 112−119.
(35) Zhong, L.; Lee, M.-Y.; Liu, Z.; Wanglee, Y.-J.; Liu, B.; Scott, S. L. *J. Catal.* **2012**, *293*, 1−12.
(36) Demmelmaier, C. A.; White, R. E.; van Bokhoven, J. A.; Scott, S. L. *J. Catal.* **2009**, *262*, 44−56.
(37) Lever, A. B. P. *Inorganic Electronic Spectroscopy*, 2nd ed.; Elsevier: Amsterdam, 1986.
(38) Budnyk, A.; Damin, A.; Barzan, C.; Groppo, E.; Lamberti, C.; Bordiga, S.; Zecchina, A. *J. Catal.* **2013**, *308*, 319−327.
(39) Perry, C. C.; Li, X. C. *J. Chem. Soc., Faraday Trans.* **1991**, *87*, 761−766.
(40) Komura, H.; Sekinobu, M. *J. Phys. Soc. Jpn.* **1970**, *29*, 1100−1100.
(41) Pappalardo, R.; Dietz, R. E. *Phys. Rev.* **1961**, *123*, 1188−1203.
(42) Mirov, S. B.; Fedorov, V. V.; Martyshkin, D.; Moskalev, I. S.; Mirov, M.; Vasilyev, S. *IEEE J. Sel. Top. Quantum Electron.* **2015**, *21*, 1−19.
(43) Espelid, Ø.; Børve, K. J. *Catal. Lett.* **2001**, *75*, 49−54.
(44) Dines, T. J.; Inglis, S. *Phys. Chem. Chem. Phys.* **2003**, *5*, 1320−1328.
(45) Moisii, C.; Curran, M. D.; van de Burgt, L. J.; Stiegman, A. E. *J. Mater. Chem.* **2005**, *15*, 3519−3524.
(46) Moisii, C.; van de Burgt, L. J.; Stiegman, A. E. *Chem. Mater.* **2008**, *20*, 3927−3935.
(47) Galeener, F. L.; Leadbetter, A. J.; Stringfellow, M. W. *Phys. Rev. B: Condens. Matter Mater. Phys.* **1983**, *27*, 1052−1078.
(48) Sen, P. N.; Thorpe, M. F. *Phys. Rev. B* **1977**, *15*, 4030−4038.
(49) Balk, R. W.; Snoeck, T.; Stufkens, D. J.; Oskam, A. *Inorg. Chem.* **1980**, *19*, 3015−3021.
(50) Balk, R. W.; Stufkens, D. J.; Oskam, A. *Inorg. Chim. Acta* **1978**, *28*, 133−143.
(51) Staal, L. H.; Terpstra, A.; Stufkens, D. J. *Inorg. Chim. Acta* **1979**, *34*, 97−101.
(52) Guzman, J.; Gates, B. C. *J. Chem. Soc., Dalton Trans.* **2003**, 3303−3318.
(53) Kirlin, P. S.; Van Zon, F. B. M.; Koningsberger, D. C.; Gates, B. C. *J. Phys. Chem.* **1990**, *94*, 8439−8450.
(54) Sholl, D. S.; Steckel, J. A. *Density Functional Theory*; 1st ed.; John Wiley & Sons: Hoboken, NJ, 2009.
(55) Duan, X.; Liu, J.; Wang, X.; Jiang, H. *Opt. Mater.* **2014**, *37*, 854−861.
(56) Deva Prasad Raju, B.; Lakshmana Rao, J.; Narasimhulu, K. V.; Gopal, N. O.; Sunandana, C. S. *Spectrochim. Acta, Part A* **2005**, *61*, 2195−2198.
(57) Arsene, J.; Lopitaux, J.; Drifford, M.; Lenglet, M. *Phys. Status Solidi A* **1979**, *52*, K111−K114.
(58) Conley, M. P.; Delley, M. F.; Siddiqi, G.; Lapadula, G.; Norsic, S.; Monteil, V.; Safonova, O. V.; Copéret, C. *Angew. Chem., Int. Ed.* **2014**, *53*, 1872−1876.
(59) Fong, A.; Yuan, Y.; Ivry, S.; Scott, S. L.; Peters, B. *ACS Catal.* **2015**, *5*, 3360−3374.
(60) Hassan, A. K.; Pardi, L. A.; Krzystek, J.; Sienkiewicz, A.; Goy, P.; Rohrer, M.; Brunel, L. C. *J. Magn. Reson.* **2000**, *142*, 300−312.

DOI: 10.1021/acscatal.5b00927
ACS Catal. 2015, 5, 5574−5583